CHINA FOUNDRY Research & Development
Vol. 23 No. 6 November 2026
www.springer.com/41230
https://doi.org/10.1007/s41230-026-4227-1

Coupling effect of Nb and BN on microstructural evolution and mechanical properties of TiAl alloy

***Zhan-xing Chen[1, 4], Zhe Deng[1, 4], Yu-peng Wang[2], **Teng-fei Ma[2], Xin-fang Zhang[1, 4], Ya-jun Yin[3], and Jian-xin Zhou[3]**

1. School of Materials Science and Engineering, Zhengzhou University of Aeronautics, Zhengzhou 450046, China
2. Key Laboratory of Air-driven Equipment Technology of Zhejiang Province, Quzhou University, Quzhou 324000, Zhejiang, China
3. State Key Laboratory of Materials Processing and Die & Mould Technology, Wuhan 430074, China
4. Collaborative Innovation Center of Processing and Detecting for Aerospace High Performance Materials, Zhengzhou 450046, China

Copyright © 2026 Foundry Journal Agency

Abstract: To improve mechanical properties of high-Nb TiAl alloys, boron nitride (BN) reinforcement was introduced, and an optimum Nb content was determined. Ti46Al2Cr0.5BN-*x*Nb (at.%) alloys were fabricated through vacuum arc melting. The microstructural evolution of Ti46Al2Cr0.5BN-*x*Nb alloys was studied, including lamellar colony size, lamellar spacing, element distribution, and the characteristics of borides and nitrides. Results show that when Nb content increases from 0 to 8at.%, the lamellar colony size of Ti46Al2Cr0.5BN-*x*Nb alloys is refined from 49 μm to 28 μm, and the lamellar spacing decreases from 463 nm to 239 nm. The increase of Nb content leads to an increase in the volume fraction of TiB_2 precipitates and a concomitant decrease in the volume fraction of Ti_2AlN precipitates. The compression strength at 800 °C shows an increase from 1,062 MPa to 1,658 MPa as the Nb content increases from 0 to 8at.%. The dominant fracture mechanisms of TiAl composites were revealed, including grain boundary fracture, crack deflection, interlamellar fracture, and pull-out of reinforcing phases.

Keywords: TiAl alloy; composite; microstructure; BN reinforcement; high-Nb TiAl alloys; mechanical properties

CLC numbers: TG146.23 **Document code:** A **Article ID:** 1672-6421(2026)06-868-09

1 Introduction

TiAl alloys are increasingly utilized in the aerospace sector due to their favorable properties such as low density, high melting temperature, superior high-temperature oxidation resistance, and notable specific strength at elevated temperatures[1-4]. The pioneering application of TiAl alloys (Ti-48Al-2Cr-2Nb) in commercial aviation was realized in the GEnx™ engine, which incorporated these materials in its low-pressure turbine (LPT) blades. This was followed by the adoption of Ti-43.5Al-4Nb-1Mo-0.1B (TNM) alloys for LPT blades in the PW1100G™ engines[5]. However, the broader engineering application of TiAl alloys is limited due to their insufficient mechanical properties at both high and ambient temperatures[6, 7].

Studies have shown that alloying can improve the mechanical properties and service temperature of TiAl alloys[8, 9]. High-Nb TiAl alloys are known for their high strength and increased service temperature, representing a new generation of TiAl alloys[10, 11]. Kim et al.[12] introduced a β-γ TiAl alloy within the chemical composition of Ti-(42–45)Al-(2–8)Nb-(1–9)(Cr, V, Mn, Mo)-(0–0.5)(B, C), featuring a high volume fraction of β-phase, which showed a fine fully lamellar structure and enhanced deformability at high temperatures. Fang et al.[13] developed the Ti46Al2.6C-*x*Nb alloys using vacuum arc melting assisted by ultrasound, in which documented an increment in strength from 2,074 MPa to 2,474 MPa and the strain from 23% to 28% as Nb content increased from 0 to 4at.%. However, the ductility of the Nb-rich TiAl alloys remains suboptimal at room temperature[14]. To counteract this, the introduction of interstitial elements like B, N, and C to refine the lamellar structure of TiAl alloys has been recommended

***Zhan-xing Chen**

Ph. D., Associate Professor. His research interests primarily focus on the design and optimization of advanced high-temperature structural materials including Ti and TiAl alloys for aerospace. To date, he has published over 20 papers in SCI indexed journals. He hosted a project funded by the National Natural Science Foundation of China and led two projects of the Science and Technology Key Project of Henan Province.

E-mail: zxchen_hit@zua.edu.cn

****Teng-fei Ma**

E-mail: matengfeihit@163.com

Received: 2024-10-19; Revised: 2025-04-07; Accepted: 2025-07-11

to optimize their mechanical attributes[15-17]. Wang et al.[18] utilized spark plasma sintering (SPS) to fabricate Ti_2AlC/TiAl composites with a network architecture, discovering that their elevated-temperature strength was significantly enhanced due to the synergistic effect of micro-Ti_2AlC and submicro-Ti_2AlC particles during compressive deformation. Kang et al.[19] prepared a Ti-48Al-2Cr-2Nb-based composite with uniformly distributed nano-micro Ti_2AlC through powder metallurgy and multiple solution-aging treatments, enhancing its properties in the heat-treated state by refining and dispersing agglomerated Ti_2AlC precipitates. Zhu et al.[20] designed Ti_2AlC/TiAl composites with refined microstructures using Ti-45Al-8Nb powder and CNTs, enhancing mechanical properties and reducing friction and wear, attributed to network-like Ti_2AlC particles. According to Yang et al.[21], the morphology of borides depends on the boron concentration, and borides of different morphologies have varying effects on the material's properties. Li et al.[22] innovatively designed a novel quasi-continuous network reinforced structure in B_4C/TiAl matrix composites, consisting of stripe- and needle-like TiB and Ti_2AlC particles. The Ti_2AlC nucleates and grows on TiB cores, stabilizing the network and enhancing the composites' high-temperature properties. As evidenced by Tan et al.[23], boron nitride addition to Ti46Al4Nb1Mo significantly reduced the average lamellar colony size from 358 μm to 49 μm and bolstered the compressive strength from 1,961 MPa to 2,493 MPa. The interstitial elements like B, N, and C are benefit to the mechanical properties of TiAl alloys, while the large size boride and carbide are detrimental to ductility. Moreover, the improvements of mechanical property for TiAl alloy have reached a bottleneck, and how to break this bottleneck is a challenge.

This study aims at improving the mechanical properties of high-Nb TiAl alloy by addition of BN, introducing a Nb-tailored, particle-reinforced TiAl composite manufactured via vacuum arc melting. The introduction of BN can not only refines the grain structure through partial dissolution of B and N into the matrix, but also promotes the formation of borides and nitrides, thereby enhancing the reinforcement of the TiAl composite. Comprehensive microstructural analyses were carried out, detailing variations in lamellar colony size, lamellar spacing, distribution of elements, and the formation of reinforcement phases. Moreover, compressive properties were assessed at elevated temperatures, accompanied by detailed fracture morphology studies. The study provides a deep understanding of the interplay between microstructure and mechanical behavior, elucidating the reinforcing and toughening mechanisms operative in TiAl composites.

2 Experimental methods

Ti46Al2Cr0.5BN-*x*Nb alloys (*x*=0, 1, 2, 4, 6, 8, in at.%) were prepared by vacuum arc melting. The raw materials were high purity titanium sponge (99.7%), aluminum (99.99%), niobium (99.98%), chromium (99.98%), and BN nanosheets (98%). The melting was carried out under a high-purity argon atmosphere, with the electrical current methodically reduced to zero in alignment with established process parameters to counteract any impact on microstructure. Each sample underwent five remelting repeats to ensure the homogeneous chemical composition, resulting in the button ingots with a diameter of 40 mm and a height of 15 mm.

The phase analysis of Ti46Al2Cr0.5BN-*x*Nb alloys was performed using X-ray diffractometry with monochromatic Cu Kα radiation in the range of 20°–90° at 5°·min^{-1}. Optical microscopy (OM, IE500M) and field emission scanning electron microscopy (SEM, Hitachi SU8010) facilitated microstructural examination, while energy dispersive X-ray spectroscopy (EDS) and transmission electron microscopy (TEM, FEI Tecnai G2 F30) enabled detailed compositional and microstructural analysis. The sample was mechanical ground to a #2000-grit finish, followed by mechanical polishing, and subsequently etched using Kroll's reagent (5% HF+10% HNO_3 +85% H_2O, vol.%). TEM specimens were wire-electrode cut and subsequently thinned to a thickness below 50 μm. Electropolishing was then performed using an automated twin-jet technique with a dual-jet electrolyte comprising a ratio of 6:3:1 for CH_3OH, $CH_3(CH_2)_3OH$, and $HClO_4$. The TEM characterization included bright field imaging (BF), EDS, and selected area electron diffraction (SAED). Statistical analyses were performed using Nano Measurer and ImageJ software, and five representative optical microscopy images were selected for each sample. Compression specimens were cylindrical with sizes of Φ5 mm×7.5 mm, sourced from the central of ingots. Compression tests were conducted on an MTS 370.10 system at elevated temperatures of 800 °C and 850 °C, maintaining a constant strain rate of 0.001 s^{-1}. Prior to deformation, specimens were thermally stabilized at target temperature for 5 min to ensure thermal equilibrium. Immediately after hot compression, the specimens were water-quenched to preserve the high-temperature microstructure for subsequent characterization.

3 Results and discussion

3.1 Microstructure of Ti46Al2Cr0.5BN-*x*Nb alloys

The as-cast Ti46Al2Cr0.5BN-*x*Nb alloys exhibit a fully lamellar microstructure, as illustrated in Fig. 1. A discernible trend is observed where the dimensions of the α_2/γ lamellar colony progressively diminish with increasing Nb content.

The BSE micrographs of the Ti46Al2Cr0.5BN-*x*Nb alloys are depicted in Fig. 2, revealing the impact of Nb content on the microstructure. Without Nb, the microstructure of TiAl alloy is composed of uniformly distributed fully-lamellar, featuring curved TiB_2 and short-rod Ti_2AlN. Following addition of 2at.% Nb, the TiAl alloy sustains the fully-lamellar structure. However, the TiB_2 morphology begins to elongate, and transitions to short strips at a Nb concentration of 6at.%. At the same time, the B2 phase content increases significantly; its volume fraction increases with an increase in Nb. It can

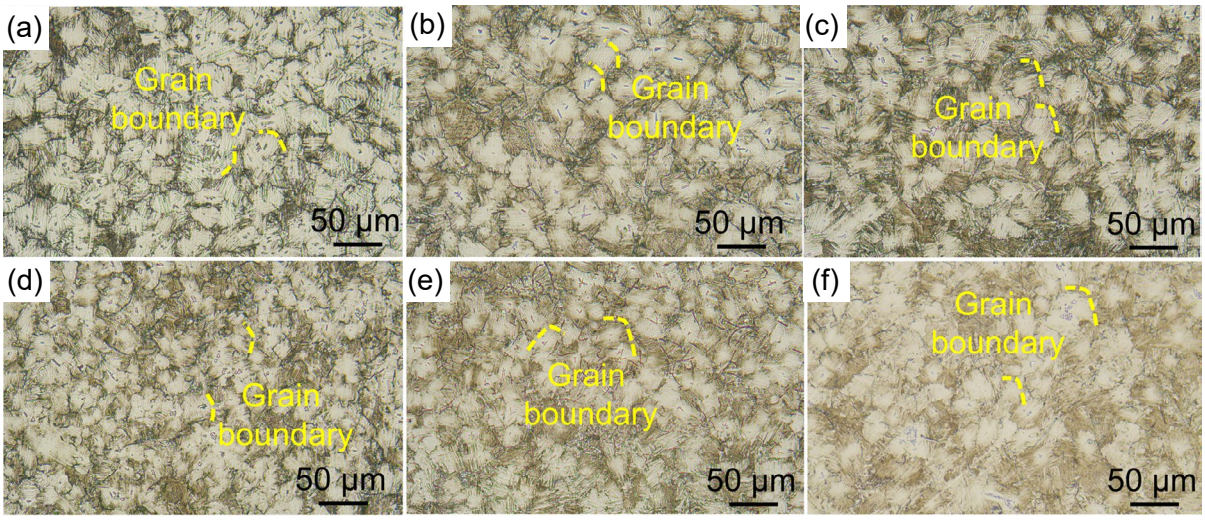


Fig. 1: OM images of Ti46Al2Cr0.5BN-*x*Nb alloys: (a) 0; (b) 1at.%; (c) 2at.%; (d) 4at.%; (e) 6at.%; (f) 8at.%

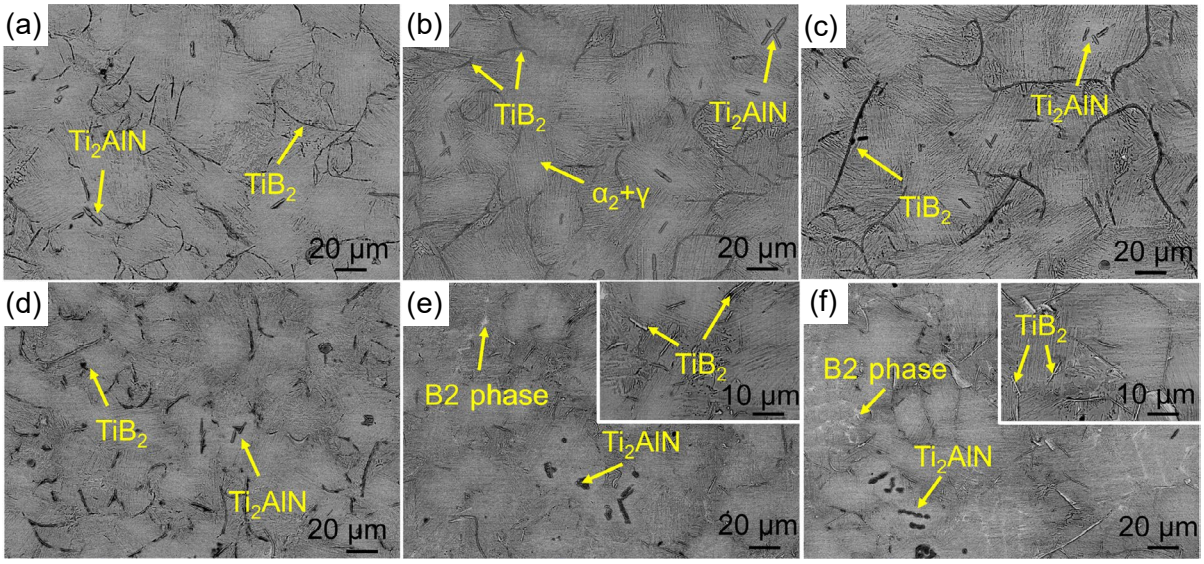


Fig. 2: BSE images of Ti46Al2Cr0.5BN-*x*Nb alloys: (a) 0; (b) 1at.%; (c) 2at.%; (d) 4at.%; (e) 6at.%; (f) 8at.%

be seen in Fig. 2(f) that Ti_2AlN appears to be significantly agglomerated. Integrating observations from Figs. 1 and 2, it is apparent that the volume fraction of TiB_2 increases with the increase of Nb, while Ti_2AlN is reduced. The rationale behind these changes lays in the β-phase stabilizing element of Nb, which expands the β-phase field and alters the balance between α_2-Ti_3Al and γ-TiAl phases[8].

In-depth analysis of elemental distribution and phase constitution for the Ti46Al2Cr0.5BN-*x*Nb alloys was conducted through EDS, with the analysis locations specified in Fig. 3 and the detailed results listed in Table 1. The energy spectrum evaluations at Points 1, 6, 9, and 11 identify a Ti to B ratio approximating 1:2, denoting the TiB_2 phase, along with a solid solution of Nb and Cr within this phase. Points 3, 4, 7, and 10 yield elemental ratios reflecting Ti, Al, and N in the proportions of 2:1:1, denoting the Ti_2AlN phase. Furthermore, a notable increase in Nb and Cr elements is observed in the bright field at Point 13, suggesting the existence of B2 phase, as opposed to the findings at Point 12, as shown in Fig. 3(d).

To gain a deeper understanding of the Ti46Al2Cr0.5BN-8Nb alloy, a TEM analysis was conducted to examine its microstructure. The results, depicted in Fig. 4, reveal a distinct and pristine interface between the precipitated phase and the matrix, with no discernible presence of additional reactants. Selected area electron diffraction (SAED) analysis was performed on the boride, nitride, and B2 phases, and the results are shown in Figs. 4(e) and (f), respectively. The γ and α_2 in the lamellar colonies follow the orientation relationship of $[010]\gamma//[0\bar{4}0]\alpha_2$ according to the SAED patterns in Fig. 4(d). Based on the FFT diffractogram in Fig. 4(i), the boride can be further identified as TiB_2.

The microstructural characteristics of Ti46Al2Cr0.5BN-*x*Nb alloys, specifically lamellar colony size, lamellar spacing, and the volume fraction of TiB_2 and Ti_2AlN phases, were evaluated using Nano Measure and ImageJ software, as presented in Fig. 5. When the Nb content increases from 0 to 8at.%, the lamellar colony is significantly refined from 49 μm to 28 μm, and the lamellar spacing decreases from 463 nm to 239 nm. The volume fraction of TiB_2 phase experiences an increase from 6.4% to 8.5%, while the Ti_2AlN phase shows a decrease

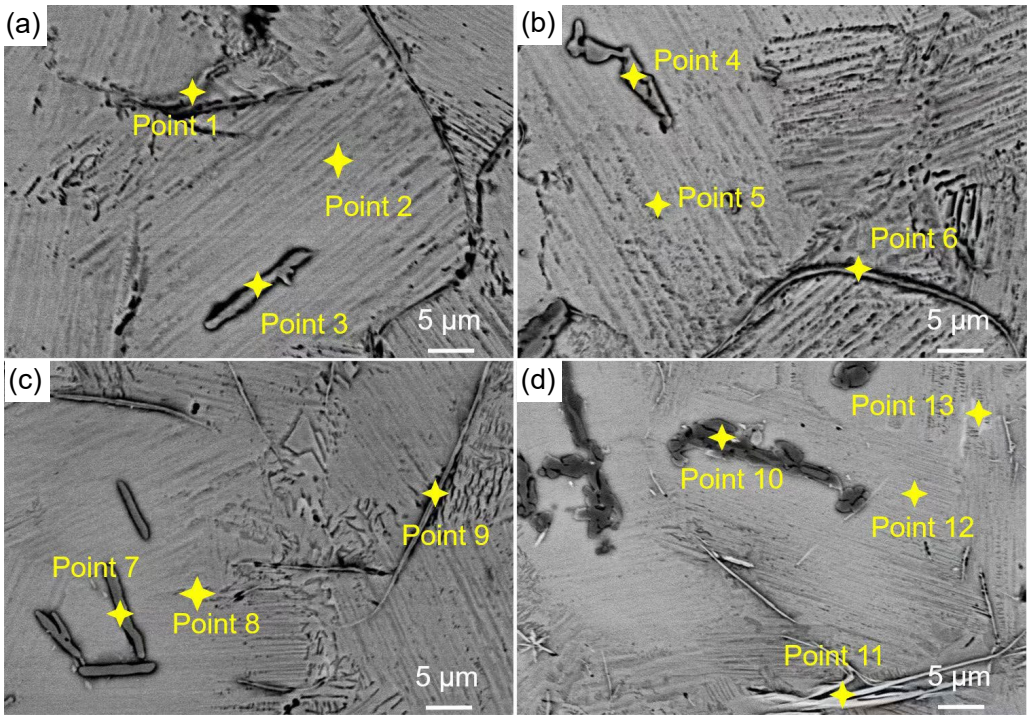


Fig. 3: EDS analysis of Ti46Al2Cr0.5BN-*x*Nb alloys: (a) 0; (b) 1at.%; (c) 4at.%; (d) 8at.%

Table 1: EDS results of Ti46Al2Cr0.5BN-*x*Nb alloys (at.%) in Fig. 3

Points	Ti	Al	Nb	Cr	N	B
1	27.69	20.98	0	1.69	0	49.64
2	51.82	46.03	0	2.15	0	0
3	45.76	24.23	0.24	1.12	28.65	0
4	47.79	26.35	0.41	0.98	24.47	0
5	51.92	45.51	1.18	1.39	0	0
6	28.71	10.31	0.44	0.85	0	59.69
7	48.25	28.01	0.37	0.64	22.73	0
8	49.37	46.24	2.89	1.5	0	0
9	22.66	10.35	1.69	1.26	6.02	58.02
10	51.12	27.23	0.86	0.44	20.35	0
11	25.6	11.75	4.5	1.13	0	57.02
12	42.73	46.05	5.24	1.9	0	4.08
13	39.31	35.7	5.81	7.03	6.14	6.01

from 3.6% to 1.5%. These results demonstrate that Nb element has the capacity to refine the lamellar structure and adjust the phase content. This can be attributed to its contribution to compositional supercooling and its role as a nucleation facilitator.

Figure 6 showcases the XRD patterns of the Ti46Al2Cr0.5BN-*x*Nb alloys, delineating the predominant diffraction peaks of the γ-TiAl and α_2-Ti_3Al phases, alongside those of the TiB_2 and Ti_2AlN phases. An assessment of the XRD results demonstrates that an increase in Nb content leads to a slight reduction in the γ phase peak intensities and an elevation in the α_2 phase peaks. Additionally, the Nb element is a strong β phase stabilizing element, contributing to the formation of B2 phase at room temperature via the ordered transformation of β phase. The absence of discernible B2 phase diffraction peaks can be ascribed to its content being below the XRD detection threshold. It has been documented that Nb exhibited a high solid solubility in TiAl[24], with the majority of Nb in the Ti46Al2Cr0.5BN-*x*Nb alloys dissolved in the α_2 and γ phases, and a smaller fraction associated with the B2 phase, which resulted from the ordered transformation of β phase.

Niobium (Nb) is a β-phase stabilizing element, thus the incorporation of Nb widened the β phase region. This augmentation in turn broadens the solid-liquid two-phase region, promoting the nucleation and subsequent growth of primary phase (β phase). According to Chen et al.[25],

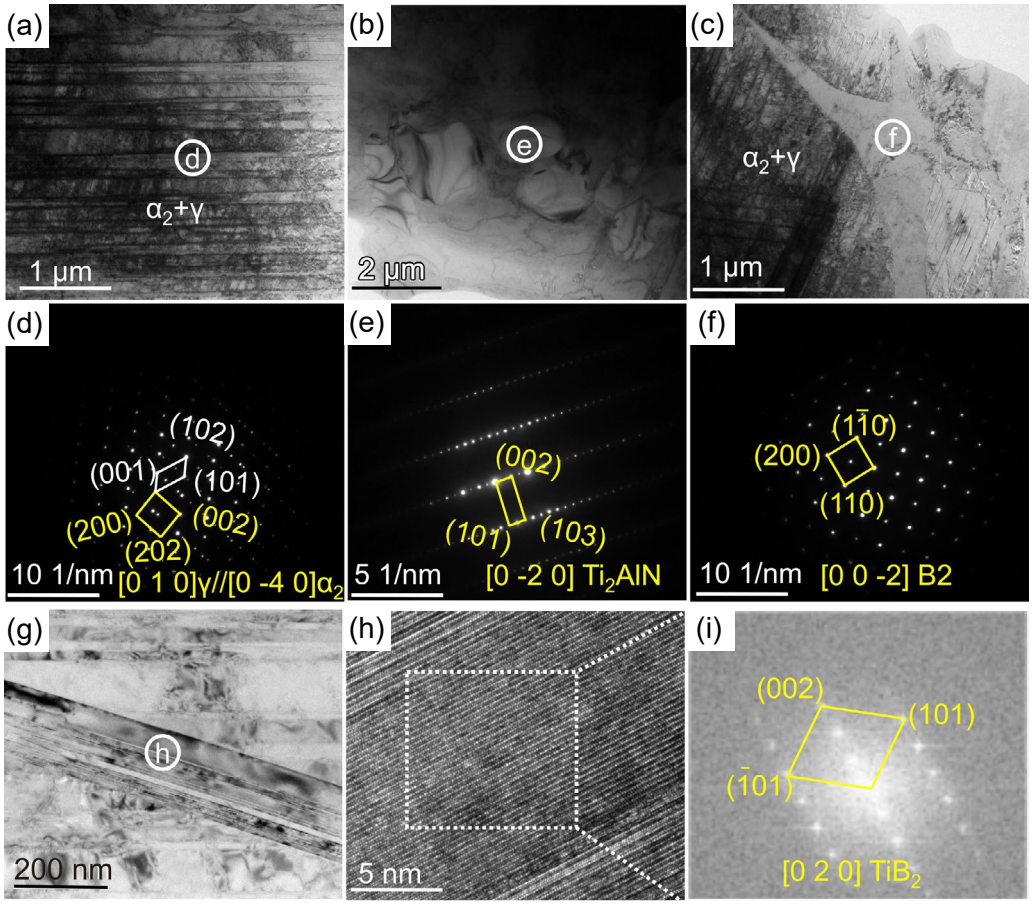


Fig. 4: TEM characterizations of Ti46Al2Cr0.5BN-8Nb composite: (a), (b) and (c) BF image; (d) SAED of (a); (e) SAED of (b); (f) SAED of (c); (g) BF image; (h) HRTEM of (g); (i) showing the corresponding FFT diffractograms

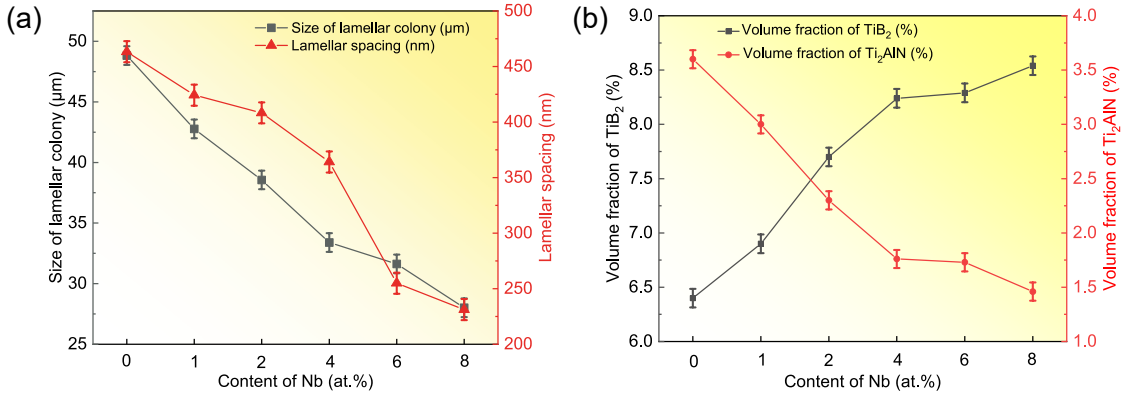


Fig. 5: Statistics results of lamellar colony size and lamellar spacing (a) and volume fraction of TiB_2 and Ti_2AlN (b) in Ti46Al2Cr0.5BN-*x*Nb alloys

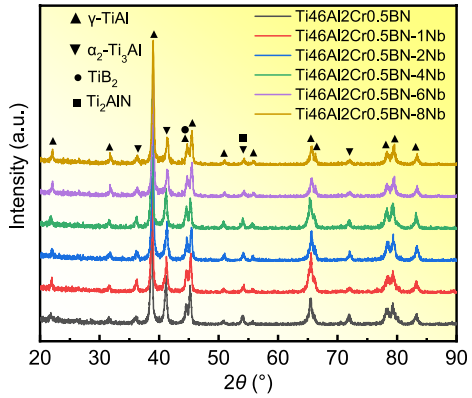


Fig. 6: XRD patterns of Ti46Al2Cr0.5BN-*x*Nb alloys

the Nb element markedly expands the β phase region, while simultaneously lowering both the α-phase transition temperature and the α→γ phase transformation temperature (T_α). As a result, increasing Nb content decreases the T_α and delays the α→γ phase transformation during solidification, resulting in a decrease of γ phase content. This is evidenced by a corresponding decrease in the diffraction peak intensity of the γ phase in the XRD patterns. The β phase is the primary phase during the solidification process, and then L+β transforms to the α phase. The Nb element is rejected at the front of solid-liquid interface, leading to constitutional subcooling and promoting the nucleation of new grains, and

therefore refines the grain size. The constitutional subcooling effect is accelerated with increasing Nb content[25].

The characteristic lamellar structure in TiAl alloys is attributed to the γ phase precipitating from the α phase, described by the reaction $\alpha \rightarrow \alpha_2+\gamma$[26]. Factors such as the precipitation rate of the γ lamellae and the time spent within the α+γ phase region significantly affect the lamellar spacing[27]. The α-phase lamellae possess a finite initial thickness prior to phase transformation, and thus the overall lamellar spacing is influenced by the number density of γ-phase lamellae. Typically, an increase in the number of γ lamellae results in a refinement of the interfacial spacing, leading to a decrease in the average lamellar spacing. With addition of Nb element, there is a reduction in the size of lamellar colonies (Fig. 1), thereby increasing the density of interfaces and providing more sites for γ phase nucleation. Consequently, the introduction of Nb element can decrease the lamellar spacing by increasing γ phase nucleation. As a β-stabilizing element, Nb shifts the solidification path toward lower Al compositions, thereby shortening the residence time within the α+γ phase region and further contributing to lamellar refinement. Furthermore, according to the TiAl phase diagram[28], the content of the α_2 and γ phases in the alloy changes when the solidification path of the alloy is biased in the low-Al direction, so the addition of Nb element also modifies the ratio of α_2 to γ phases. Chu et al.[29] found that the content of Ti_3Al phase and TiAl phase affects the content of Ti_2AlN phase due to the different solubility of element N in these two phases. Moreover, considering the different solubilities of B and N in α_2 to γ phases, the proportions of TiB_2 and Ti_2AlN phases are modulated in response to variations in Nb content[30, 31].

Figure 7 shows the detailed microstructure evolution mechanism of the Ti46Al2Cr0.5BN-*x*Nb alloys. At 0at.% Nb, the matrix contains Ti_2AlN and TiB_2 phases, with coarse lamellar colony sizes and wide interlamellar spacings. When Nb (1at.%–4at.%) is added, it discharges to the solidification front, inducing constitutional subcooling, which refines both the lamellar colony size and spacing. With a further increase in Nb content (6at.%–8at.%), the lamellar colonies and spacings are further refined, and the B2 phase appears in the matrix.

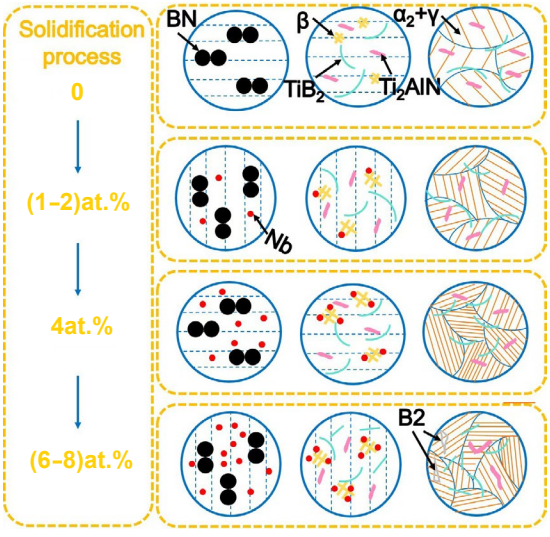


Fig. 7: Microstructural evolution diagram of Ti46Al2Cr0.5BN-*x*Nb alloys

3.2 Compressive properties of Ti46Al2Cr0.5BN-*x*Nb alloys

The high-temperature compression stress-strain relationships for the Ti46Al2Cr0.5BN-*x*Nb alloys are depicted in Fig. 8. As indicated, the engineering stress is markedly influenced by the Nb content. Without Nb, the alloy demonstrates a minimum compressive strength of 1,062 MPa, whereas a peak strength of 1,658 MPa is observed at 8at.% Nb compressed at 800 °C. The high temperature compression results at 850 °C show that the strength increases from 963 MPa to 1,215 MPa as the Nb content increases from 0 to 8at.%. These data suggest that a higher Nb content is advantageous for enhancing the high-temperature strength of the Ti46Al2Cr0.5BN-*x*Nb alloys.

The increase of compressive properties is mainly affected

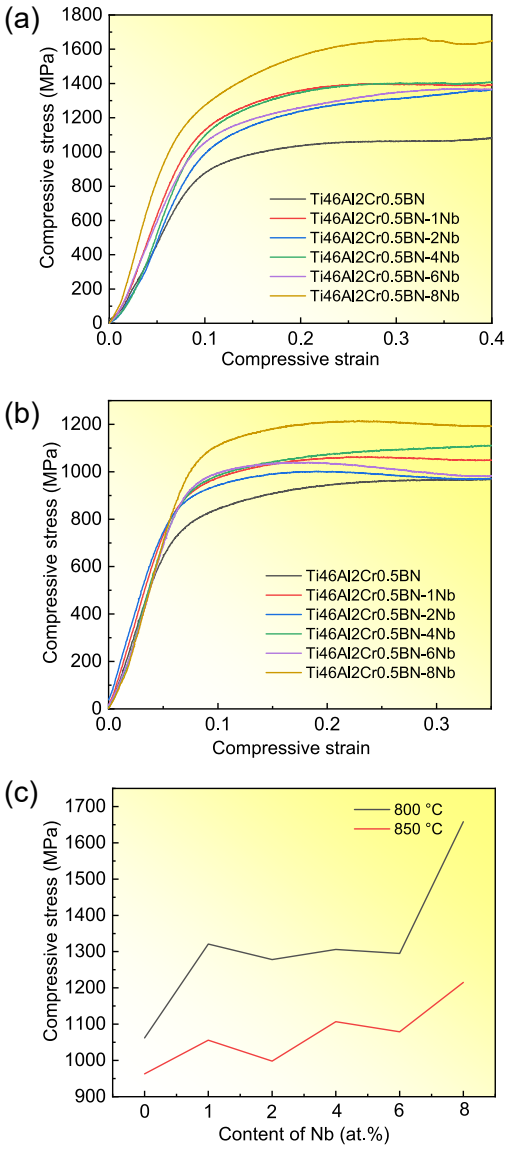


Fig. 8: Compression stress-strain curves of Ti46Al2Cr0.5BN-*x*Nb alloys deformed at high temperatures: (a) 800 °C; (b) 850 °C; (c) strength vs. Nb content curve

by the refinement of lamellar colony, solid-solution of Nb, and the precipitation strengthening of Ti_2AlN and TiB_2[3, 6]. With the increase of Nb content, the lamellar colony size and lamellar spacing are refined. The relationship between strength and grain size of TiAl alloys can be described using Hall-Petch equation[32]:

$$\sigma = \sigma_0 + Kd^{-1/2} \quad (1)$$

where σ is the strength, σ_0 is the strength without Nb addition, and K is a constant with a value of 4.8 MPa·m$^{-1/2}$ for TiAl alloy[33], and d is grain size or the lamellar spacing. The average lamellar colony size is 48.8 μm for 0at.% Nb and 28 μm for 8at.% Nb alloy (Fig. 5), therefore grain refinement strengthening $\Delta\sigma_{GB}$=220 MPa.

The Ti_2AlN and TiB_2 particles bear a certain load when the alloy is stressed, and the effect of load transfer is remarkable when the interface is coherent between the matrix and reinforcements. The shear lag model is commonly used for estimating the load transfer between the ductile matrix and hard reinforcing phase in composites[34]. The strengthening effect results from load transfer, denoted as σ_{LT}, can be expressed as:

$$\sigma_{LT} = \sigma_0 \left[\frac{1}{2} V_W \left(2 + \frac{l}{d} \right) + (1 - V_W) \right] \quad (2)$$

where σ_0 is the yield strength and V_W represents the volume fraction of the Ti_2AlN (3.6% at 0at.% Nb and 1.46% at 8at.% Nb, as shown in Fig. 5) and TiB_2 phase (6.4% at 0at.% Nb and 8.54% at 8at.% Nb, as shown in Fig. 5) in the alloy; l/d denotes the aspect ratio of the precipitate phases. Specifically, the aspect ratio of Ti_2AlN increases from 5.3 in the Nb-free alloy to 6.5 with the addition of 8at.% Nb, whereas that of TiB_2 decreases from 11 to 8 over the same compositional range. Then, the load transfer strengthening $\Delta\sigma_{LT}$ is calculated to be 126 MPa at 800 °C with 0 Nb and 117 MPa at 850 °C with 8at.% Nb.

The compressive stress-strain behavior of TiAl composites at elevated temperatures, as shown in Fig. 8, indicates the absence of a clear yielding stage across different Nb contents. During the initial stage of high-temperature deformation, a rapid increase in engineering stress with strain is observed, reflecting a pronounced work-hardening effect due to extensive dislocation activities. As deformation proceeds, the peak engineering stress is attained and subsequently reaches a plateau, which can be attributed to high-temperature dynamic recovery and recrystallization phenomena that mitigate work-hardening effects. The interplay of work-hardening and dynamic softening leads to an equilibrium in engineering stress levels. The propensity for twin formation, which is augmented at elevated temperatures, serves to improve high-temperature ductility[35]. Furthermore, the grain refinement resulting from Nb addition enhances both the strength and ductility of the alloys[36], thus improving the high-temperature strength of the Ti46Al2Cr0.5BN-*x*Nb alloys as the Nb content increases.

The high-temperature compression fracture morphology of Ti46Al2Cr0.5BN-*x*Nb alloys is displayed in Fig. 9. It reveals an absence of pronounced macroscopic cracks within the deformed matrix. However, localized microcracks are present predominantly at the lamellar colony boundaries. These microcracks are attributed to stress concentrations at grain boundaries and voids resulting from the withdrawal of second-phase particles. Additionally, fracturing and bending of precipitated phases are evident in the figure, suggesting that these phases play a role in absorbing and redistributing stress, thereby contributing to the high-temperature compressive strength. The significant elongation and bending of lamellar colonies also demonstrate the excellent high-temperature deformability of the TiAl composites across the range of Nb contents.

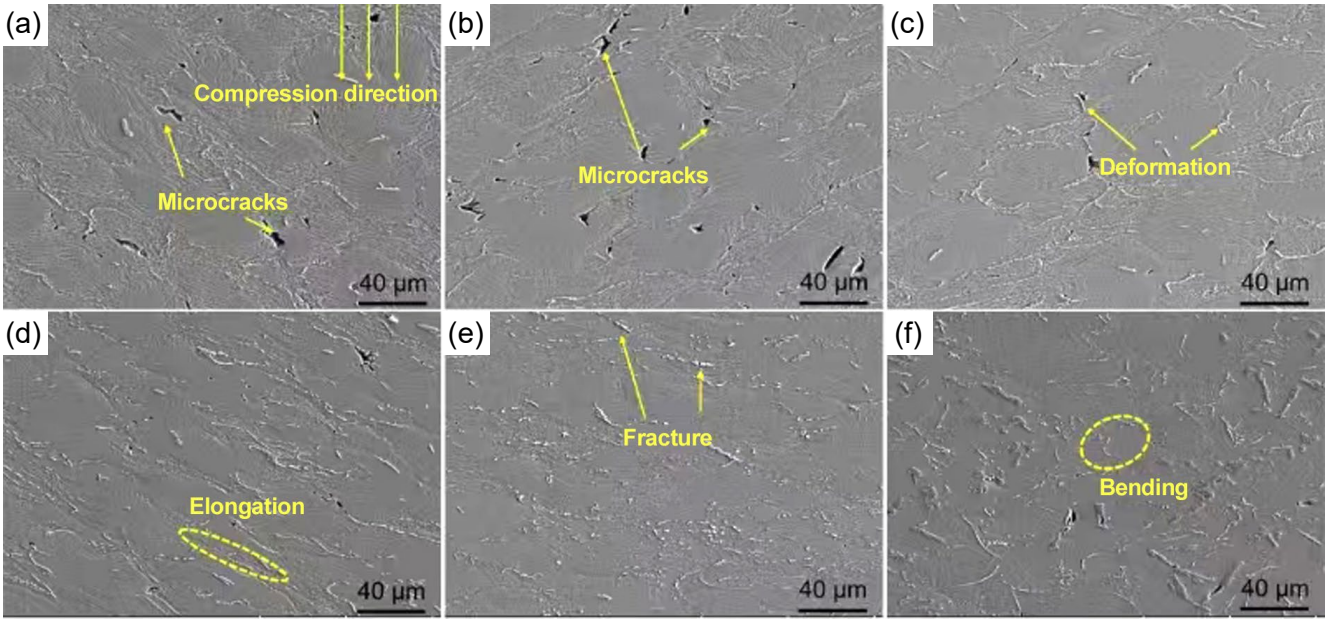


Fig. 9: Deformation microstructures of Ti46Al2Cr0.5BN-*x*Nb alloys deformed at 800 °C: (a) 0; (b) 1at.%; (c) 2at.%; (d) 4at.%; (e) 6at.%; (f) 8at.%

4 Conclusions

Ti46Al2Cr0.5BN-*x*Nb alloys were fabricated utilizing the vaccum arc melting method, and their microstructural development was thoroughly investigated, concentrating on lamellar colony size, lamellar spacing, and the precipitate phases. Mechanical property assessments were performed, and the associated deformation mechanisms were analyzed, culminating in the subsequent conclusions:

(1) Variations in Nb content directly affect the volume fractions of the precipitated phases in the Ti46Al2Cr0.5BN-*x*Nb alloys. An increase in Nb content leads to a reduction in volume fraction of Ti_2AlN phase, accompanied by an increase in the TiB_2 phase. Concurrently, the TiB_2 phase undergoes a distinct morphological evolution from a curved to a strip-like morphology due to the expansion of β-phase region.

(2) Nb addition results in significant grain refinement; as Nb content increases from 0 to 8at.%, the lamellar colony size decreases from 49 μm to 28 μm, and interlamellar spacing narrows from 463 nm to 239 nm. This refinement is primarily attributed to Nb-induced subcooling and the resultant enhancement in heterogeneous nucleation.

(3) Significant improvements in high-temperature mechanical performance are achieved through Nb addition. At 800 °C, the compressive strength increases by 56% (from 1,062 MPa to 1,658 MPa) with the addition of 8at.% Nb. At 850 °C, the strength rises from 963 MPa to 1,215 MPa across the same compositional range (0 to 8at.% Nb).

(4) The enhancements in mechanical properties are attributed to the combined effects of grain refinement and solid solution strengthening. The microcrack observed within TiB_2 and Ti_2AlN particles under high-temperature stress highlights their critical role in stress absorption and redistribution.

Acknowledgments

This work was supported by the Henan Provincial Key Research and Development & Promotion Special Program (No. 251111231400); the National Natural Science Foundation of China (No. 52001283); the Natural Science Foundation of Henan (No. 252300420066); the State Key Laboratory of Materials Processing and Die & Mould Technology, Huazhong University of Science and Technology (No. P2024-017); the Youth Research Funds Plan of Zhengzhou University of Aeronautics (No. 25ZHQN01023); the Scientific Research Team Plan of Zhengzhou University of Aeronautics (No. 25ZHTD01003); and the Shaanxi Key R&D Program(No. 2025CY-JJQ-18).

Conflict of interest

The authors declare that they have no conflict of interest.

References

[1] Gu X, Jiang S D, Cao F Y, et al. A β-solidifying TiAl alloy reinforced with ultra-fine Y-rich precipitates. Scripta Materialia, 2021, 192: 55–60.

[2] Dong S L, Ding X, Chen R R, et al. High-temperature deformation resistance and creep resistance of a TiAl-based alloy fabricated by cold crucible directional solidification technology. China Foundry, 2020, 17(4): 378–383.

[3] Chen Z X, Deng Z, Wang Y P, et al. Solidification behavior of TiB_2-Ti_2AlN reinforced TiAl composites with variation Al content. Intermetallics, 2025, 178: 108640.

[4] Liu P, Hou B, Wang A Q, et al. Superior strength-plasticity synergy in a heterogeneous lamellar Ti_2AlC/TiAl composite with unique interfacial microstructure. Journal of Materials Science and Technology, 2023, 159: 21–32.

[5] Lin B C and Chen W. Mechanical properties of TiAl fabricated by electron beam meltin – A review. China Foundry, 2021, 18(4): 307–316.

[6] Deng Z, Chen Z X, Wang Y P, et al. In-situ synthesized multi-component particle reinforced TiAl composite with excellent mechanical properties. Materials Today Communications, 2024, 38: 108060.

[7] Liu P, Wang Z B, Ye F, et al. Hierarchically heterogeneous strategy for Ti_2AlC/TiAl composite with superior mechanical properties. Composites: B, 2024, 273: 111259.

[8] Yang G, Kou H C, Yang J R, et al. Microstructure control of Ti-45Al-8.5Nb-(W, B, Y) alloy during the solidification process. Acta Materialia, 2016, 112: 121–131.

[9] Lapin J, Pelachová T, and Bajana O. High temperature deformation behaviour and microstructure of cast in-situ TiAl matrix composite reinforced with carbide particles. Journal of Alloys and Compounds, 2019, 797: 754–765.

[10] Chen G, Peng Y B, Zheng G, et al. Polysynthetic twinned TiAl single crystals for high-temperature applications. Nature Materials, 2016, 15: 876–881.

[11] Zhang W J, Deevi S C, and Chen G L. On the origin of superior high strength of Ti-45Al-10Nb alloys. Intermetallics, 2002, 10: 403–406.

[12] Kim Y W, Kim S L, Dimiduk D, et al. Development of beta gamma alloys: Opening robust processing and greater application potential for TiAl-base alloys. In: Proceedings of Gamma Titanium Aluminides, 2008: 215.

[13] Zhou L Y, Fang H Z, Chen R R, et al. Effects of niobium and ultrasonic action coupling on microstructure evolution and mechanical properties of Ti46Al2.6C alloy. Journal of Alloys and Compounds, 2022, 904: 164048.

[14] Wang Q, Chen R R, Yang Y H, et al. Effects of V and B, Y additions on the microstructure and creep behaviour of high-Nb TiAl alloys. Journal of Alloys and Compounds, 2018, 747: 640–647.

[15] Liu Y W, Hu R, Yang J R, et al. Tensile properties and fracture behavior of in-situ synthesized Ti_2AlN/Ti48Al2Cr2Nb composites at room and elevated temperatures. Materials Science and Engineering: A, 2017, 679: 7–13.

[16] Wang L, Gabrisch H, Lorenz U, et al. Nucleation and thermal stability of carbide precipitates in high Nb containing TiAl alloys. Intermetallics, 2015, 66: 111–119.

[17] Liu B, Li J, Hu D W. Solidification and grain refinement in Ti(48–50)Al2Mn2Nb1B alloys. Intermetallics, 2018, 101: 99–107.

[18] Wang Z B, Liu P, Wang A Q, et al. Fabrication, microstructure and mechanical properties of TiAl matrix composite reinforced by submicro/nano-Ti_2AlC. Materials Characterization, 2023, 203: 113141.

[19] Kang X, Pu Z N, Zheng M M, et al. Optimization of microstructure and high-temperature mechanical properties of Ti4822/Ti_2AlC composites through multiple solution-aging treatments. Journal of Alloys and Compounds, 2024, 1008: 176862.

[20] Zhu D D, Yan J F, Wang Y P, et al. Enhancing the mechanical and tribological properties of TiAl alloy by network structured Ti_2AlC. Journal of Materials Science, 2024, 59: 5399–5413.

[21] Yang C, Jiang H, Hu D, et al. Effect of boron concentration on phase transformation texture in as-solidified Ti44Al8NbxB. Scripta Materialia, 2012, 67: 85–88.
[22] Li M A, Yang W G, Li J, et al. Microstructures and mechanical properties of TiAl matrix composites with multi-precipitates quasi-continuous network reinforced structures. Materials Science and Engineering: A, 2024, 901: 146573.
[23] Tan Y M, Chen R R, Liu Y L, et al. Formation of Ti_2AlN and TiB and its effect on mechanical properties of Ti46Al4Nb1Mo alloy by adding BN particles. Materials Science and Engineering: A, 2019, 756: 161–171.
[24] Fang H Z, Chen R R, Yang Y, et al. Effects of tantalum on microstructure evolution and mechanical properties of high-Nb TiAl alloys reinforced by Ti_2AlC. Research, 2020(1): 194–204.
[25] Chen G L, Xu X J, Teng Z K, et al. Microsegregation in high Nb containing TiAl alloy ingots beyond laboratory scale. Intermetallics, 2007, 15(5–6): 625–631.
[26] Denquin A and Naka S. Phase transformation mechanism involved in two-phase TiAl-based alloys – I. Lamellar structure formation. Acta Materialia, 1995, 43: 343–349.
[27] Tang J C, Huang B Y, Zhou K C, et al. Effect of Al content on the lamellar spacing in two-phase TiAl alloys. Journal of Materials Science Letters, 2001, 20: 1863–1864.
[28] Okamoto H. Al-Ti (aluminum-titanium). Journal of Phase Equilibria and Diffusion, 2000, 3: 311.
[29] Chu C L and Wu S K. Ion nitriding of titanium aluminides with (25–53)at.% Al. I: Nitriding parameters and microstructure characterization. Surface & Coatings Technology, 1996, 78: 211–218.
[30] Larson D J, Liu C T, and Miller M K. Boron solubility and boride compositions in $\alpha_2+\gamma$ titanium aluminides. Intermetallics, 1997, 5(6): 411–414.
[31] Kaufman M J, Konitzer D G, Shull R D, et al. An analytical electron microscopy study of the recently reported "Ti_2Al phase" in γ-TiAl alloys. Scripta Metallurgica, 1986, 20: 103–108.
[32] Sen I, Tamirisakandala S, Miracle D B, et al. Microstructural effects on the mechanical behaviour of B-modified Ti-6A1-4V alloys. Acta Materialia, 2007, 55: 4983–4993.
[33] Yang S C, Cui C X, Cui S, et al. Ti-46Al-4Nb alloy refined and reinforced by in-situ TiC nanoparticles and TiB_2 whiskers. Journal of Alloys and Compounds, 2022, 892: 162–195.
[34] Fang H Z, Wang S, Chen R R, et al. The effects of the formation of a multi-scale reinforcing phase on the microstructure evolution and mechanical properties of a Ti_2AlC/TiAl alloy. Nanoscale, 2021, 13: 12565–12576.
[35] Chen Y Y, Li B H, and Kong F T. Effects of minor yttrium addition on hot deformability of lamellar Ti-45Al-5Nb alloy. Transactions of Nonferrous Metals Society of China, 2007, 17: 58–63.
[36] Hwang Y J, Hong S H, Kim Y S, et al. Influence of silicon content on microstructure and mechanical properties of Ti-Cr-Si alloys. Journal of Alloys and Compounds, 2018, 737: 53–57.